ACS OMEGA

http://pubs.acs.org/journal/acsodf

Article

Efficient Capture of Heavy Metal Ions and Arsenic with a CaY–Carbonate Layered Double-Hydroxide Nanosheet

Md. Hasan Zahir,* Kashif Irshad, Mohammad Mizanur Rahman, M. Nasiruzzaman Shaikh, and Mohammad Mominur Rahman

Cite This: *ACS Omega* 2021, 6, 22909–22921

Read Online

ACCESS | Metrics & More | Article Recommendations | Supporting Information

ABSTRACT: Nanosheets consisting of two-dimensional (2-D) nanomaterials made up of Ca^{2+} (Ca), and Y^{3+} (Y) cations and carbonate [CO_3^{2-}] anions in the interlayer with a uniform thickness and lengths of around 10 μm have been successfully synthesized in a hydrotalcite layer structure, otherwise known as a layered double hydroxide, using a facile hydrothermal method. The resulting CaY–CO_3^{2-} layered double-hydroxide (LDH) materials demonstrate outstanding affinity and selectivity for toxic transition metal ions such as Cr^{3+}, Ni^{2+}, Cu^{2+}, Zn^{2+}, Pb^{2+}, Cd^{2+}, and Hg^{2+} as well as metalloid As^{3+}. The adsorption of all of the highly toxic metal ions from the aqueous solution was found to be exceptionally rapid and highly selective, with more than 95% removal achieved within 30 min. For AsO_3, a strong adsorption potential of 452 mg/g was observed at pH 7.0, which is better than most values previously reported. The distribution coefficient K_d values can exceed ~10^6 mL/g for Cr^{3+}, Pb^{2+}, and As^{3+}, which are highly toxic. The fabricated materials have excellent chemical stability: they retain their well-defined lamellar shapes even under mildly acidic conditions.

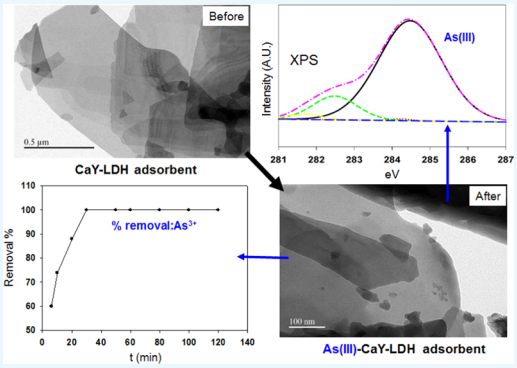

INTRODUCTION

As pollution of water is a significant environmental problem, there is an urgent need to develop new kinds of materials that can effectively eliminate toxic metal ions from drinking water.[1] There are no commercially available one-step systems and/or adsorbents for the simultaneous removal of toxic heavy metal ions and the poisonous metalloid arsenic from drinking water. Trace amounts of arsenic in drinking water are responsible for skin diseases, liver and lung cancers, additionally immune disorders, neurological diseases, nervous disorders, and disturbances in the cardiovascular system.[2] Consequently, the EPA of the USA and WHO have determined the optimum level of arsenic concentration of 0.001 mg/dL in drinking water.[3,4] Currently, 70 million people are affected by the arsenic contamination of water, particularly in the United States, Mexico, Canada, New Zealand, China, Taiwan, Argentina, Chile, Poland, Japan, Bangladesh, India, and Pakistan.[4,5]

Despite their harmful effects on humans and other living species, the presence of poisonous metals such as Hg^{2+}, Pb^{2+}, and Cd^{2+} in water is also a major environmental concern.[6] A major challenge is the production of an efficient method for extracting toxic heavy metals and arsenic from water so that they are present only at trace levels (e.g., <0.005 ppm). As a result, a water purification system must be developed that is both quick and chemically stable, as well as pH sensitive.

Many research groups have used very common materials such as polymer, carbon, biomaterials, and resins to remove toxic and/or heavy metal ions. Nonetheless, adsorption is particularly attractive using the many suggested methods due to their low cost, simple design, good operability, and high adsorbent removal efficiency.[7−15] Nanostructured materials are yet another candidate for metal ion absorption due to their high volume-to-surface ratio.[16] However, they are not effective in real applications due to their tendency to agglomerate, and it is also difficult to control their release level during the remediation process. Aziz et al. have shown that $CaCO_3$ can remove over 90% of heavy metal ions at a concentration of 2 mg/L at 8.5 pH. However, this kind of system is not viable for practical applications.[7]

Over the last decade, many LDH materials and their derived oxides (LDOs) were used to adsorb arsenate and phosphate, with a relatively large adsorption amount through anion exchange or reconstruction. Both involved anion intercalation in the interlayer spaces. Koroda et al. showed a significant anion exchange capacity of LDH-NP (NP = nanoparticles) and

Received: July 6, 2021
Accepted: August 13, 2021
Published: August 25, 2021

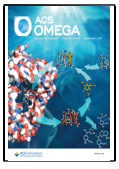

an effective reusable As, selenium, and born scavenger.[17] Wang et al. demonstrated the synergistic Pb(II) removal effect of CO_3^{2-} and OH^- derived from hydrozincite and Zn/Al−CO_3^{2-} hydrotalcite adsorbents.[18] Yu et al. have found that As(V) can be very efficiently extracted by intercalation into the interlayer of reconstructed MgAl LDHs at a concentration below 10 mg/L than 0.010 mg/L of the As remaining in the solution.[19] Xu et al. also noticed that for removing both phosphate and arsenate, the physical mixture of CaO and Fe_2O_3 with identical compositions is not as powerful as CaFe LDH. This suggests that Ca^{2+} in LDH/LDO is more efficiently used as the precipitant to remove phosphate and arsenate.[20] However, it is worth mentioning that few researchers used Ca-containing LDH materials to remove arsenate and phosphate,[20] while nobody noticed the function of these LDHs as precipitants of arsenate and phosphate, let alone the comparison of the removal efficiency between intercalation and precipitation when LDH materials were used as adsorbents. Ma et al. reported a highly selective and efficient heavy metal capture with polysulfide-intercalated layered double hydroxides.[21] Sulfides are well-known adsorbent materials for water extraction of toxic metal ions because they are capable of forming covalent bonds with heavy metals. However, sulfur can cause hyperplasia with abundant nasal secretions and dyspnea that can be streaked with blood.[21] Furthermore, precipitation methods using sulfide ions cannot reduce heavy metal concentrations below the levels required for drinking water.[21−23]

Xu et al. reported that divalent (M^{II}) and trivalent cations (M^{III}) could be used to prepare LDHs by substituting them fully or partially for Mg^{II} or Al^{II} in brucite-like layers.[24] The only requirement of the divalent and trivalent cations is that their radii for octahedral coordination must not be excessively different from Mg^{II} and Al^{III}.[25,26] The ionic radii of Ca^{2+} and Y^{3+} are 0.100 and 0.090 nm, respectively (Table 1), so it is theoretically possible to synthesize CaY-based LDHs.

Table 1. Ionic Radii of Some Cations with the Coordinate Number of 6[a],[26]

MII	radius (nm)	MIII	radius (nm)
Fe	0.061	Al	0.054
Co	0.065	Co	0.055
Ni	0.069	Fe	0.055
Mg	0.072	Mn	0.058
Cu	0.073	Ga	0.062
Zn	0.074	Rh	0.067
Mn	0.083	Ru	0.068
Pd	0.086	Cr	0.069
Cd	0.095	V	0.074
Ca	0.100	Y	0.090
Ti^{IV}	0.061	La	0.103
Sn^{IV}	0.069	Zr^{IV}	0.072

[a]Adapted with permission from ref 26. Copyright Elsevier 2021.

Still, their preparation has not previously been reported. It has been demonstrated that Y_2O_3 can be incorporated in small amounts in MgAl LDHs containing Cr^{3+}.[27] Yang et al. reported that a Y_2O_3 adsorbent prepared with the hydrothermal method exhibits a high arsenate (As(V)) adsorption capacity.[19] Recently, Zhang et al. reported a substantial increase in the removal of arsenic from aqueous solution in the presence of $CaCO_3$ and a 99.64% adsorption capacity.[28] Zhipan et al. also tested the efficiency of mesoporous Fe-Ce bimetal oxides and found an excellent percentage of arsenic removal from water.[29]

In this study, we systematically synthesized a CaY LDH nanosheet by mixing Ca^{2+} and Y_2O_3 (molar ratio of 75:25 mol %) in water and found that this method enables the preparation of micrometer-scale LDH particles that can be tailored in size and morphology. Moreover, we explored the mechanism of forming the lamellar CaY LDH structure and its dependence on the molar ratio of Ca/Y. Finally, we obtained promising results for eliminating and/or removing toxic metal and arsenic ions from water by CaY LDHs, indicating that they may have industrial uses. This contribution is expected to fill a significant research gap in the development and applications of a CaY LDH-based sorbent for water purification.

RESULTS AND DISCUSSION

Chemical Structure of the Adsorbent. The X-ray diffraction (XRD) patterns of Ca/Y with molar ratios of (a) 75:25, (b) 50:50, and (c) 25:75 samples, respectively, are shown in Figure 1. The XRD patterns for Y_2O_3 [(d)] and

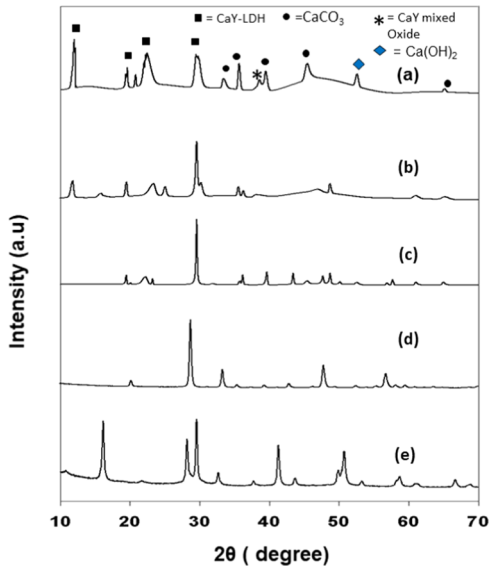

Figure 1. XRD patterns for as-synthesized CaY LDH samples with Ca/Y molar ratios of (a) 75:25, (b) 50:50, and (c) 25:75, and for (d) Y_2O_3 and (e) $Y(OH)_3$. These samples were prepared with the hydrothermal method at 200 °C and pH 8.5.

$Y(OH)_3$ [(e)] are shown for comparison. The CaY−CO_3^{2-} LDH diffraction pattern shows a distinctive layered structure with a basal *d*-value of 0.76 nm, similar to previous findings.[30] The sharp peaks suggest that the samples are crystalline; the peaks of (003), (006), (018), (012), (111), (110), and (113) planes are characteristic of layered clay minerals (LDHs).[31] The XRD patterns for the CaY−CO_3^{2-} LDHs (Figure 1a,b) are identical to those in JCPDS file No. 38-0487. Figure 1a,b shows that mixed phases are present in the LDHs. Note that LDH materials with mixed phases have been reported elsewhere.[28]

Figure 1 shows that the intensities of all peaks of the CaY LDHs decrease with increase in the proportion of Y. The low-angle diffraction peaks are indexed as (003) and (006) for a rhombohedral symmetry. They are very intense and distinct for samples (a) and (b) (prepared with molar ratios of 75:25 and 50:50 and 24 h of hydrothermal treatment). In Figure 1a, the

https://doi.org/10.1021/acsomega.1c03294
ACS Omega 2021, 6, 22909−22921

line at 2θ value characteristic for the (003) reflection of LDH was the highest of all in the diffraction pattern. Figure 1d shows that the well-defined XRD pattern for Y_2O_3 has completely disappeared in the pattern for the LDH product. One exciting feature of these samples is the production of a $3R_2$-polytype LDH step, which seldom occurs in coprecipitation synthesis.[32] In the case of MgAl−OH LDHs, the intensity of the polytype peaks decreases after long hydrothermal treatment.[23] MgAl−OH LDH preparation is very time consuming, taking 10 days of hydrothermal treatment, which means that the formation of MgAl−OH LDH requires long-term aging. In this study, a different type of reaction occurs in the LDH preparation process, i.e., the XRD peaks of CaY LDH do not persist after long hydrothermal treatment, which results in morphologies that are no longer lamellar. CaY LDHs were obtained with the same layered morphology as that of MgAl−OH LDHs after only 24 h of hydrothermal reaction. Figure 1 shows the $Ca(OH)_2$ impurity phase, which is generated simultaneously. This phase is also evident at 3720 cm^{-1} (very weak) in the Fourier transform infrared (FT-IR) spectra of samples (a), (b), and (c) in Figure 2.

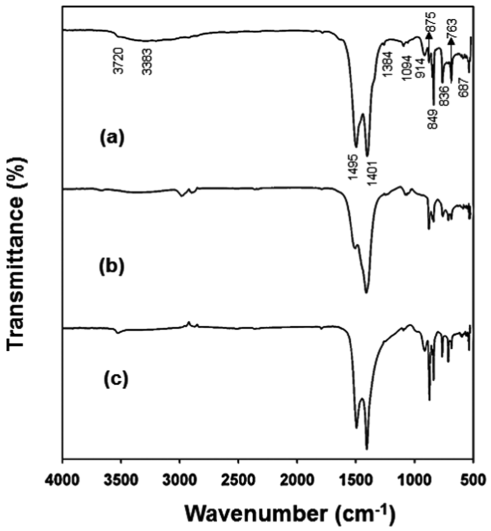

Figure 2. FT-IR spectra of as-synthesized CaY LDH samples with the Ca/Y molar ratios of (a) 75:25, (b) 50:50, and (c) 25:75.

FT-IR Analysis. The FT-IR spectra of Ca/Y with molar ratios of (a) 75:25, (b) 50:50, and (c) 25:75 for the samples are shown in Figure 2. A very weak peak near 3700 cm^{-1} can be seen for all samples due to the −OH group's vibration. Due to the antisymmetric mode of carbonate anions and/or free carbonate species, the strong band at 1401 cm^{-1} appeared.[33] Carbonate molecules occur through the chemical absorption of CO_2. This presumably occurred on the surface of the CaY−CO_3^{2-} LDH sheets throughout the collection cycle and the subsequent $CO_2 + OH^- \rightarrow HCO_3^-$ or CO_3^{2-} reaction. Typical M−O and M−OH (M = Ca, Y) vibrations in LDH materials peak at 875, 849, 836, 763, and 687 cm^{-1}.

The peak at 875 cm^{-1} is assigned to carbonate mode υ_2,[33,34] while the other two bands are assigned to carbonate mode υ_4 due to the loss of degeneration of the mode that was originally doubly degenerated. Because of the free carbonate species, the peak at 680 cm^{-1} appeared. The observed reduction in symmetry is probably due to the interactions between carbonate anions and H_2O molecules in the interlayer space and with OH groups. The weak shoulder peak at 1384 cm^{-1} appeared probably due to the NO_3^- group.

Morphology Characterization. In this study, we examined the role of varying the Y and Ca contents for a constant pH, reaction time, and temperature in LDH formation. Sheet-like layer structures start to form when the molar ratio of Y is higher than that of Ca, as shown in Figure 3a. Ca−Y−CO_3^{2-} LDH sheet-like crystallites form for a Ca/Y molar ratio of 75:25. Such as-prepared LDHs, as can be seen in the scanning electron microscopy (SEM) images in Figure 3a, are composed on average of larger crystallites with a lateral dimension above 1 μm. In the CaY−CO_3 LDH obtained after 24 h hydrothermal treatment, rectangular crystallites with lateral dimensions of 1−5 μm are formed (Figure 3a). For LDH materials, such large CaY−CO_3^2 LDH crystallites can be seen in the red ring in Figure 3a. To the best of our understanding, LDH is made up of Ca, and Y has not been reported in the literature before. A similar morphology occurs for MgAl−CO_3^2, with a lateral dimension of 1−3 μm, but 10 days of calcination is needed.[35] When the Ca and Y content is 50:50 mol %, the pineapple particles are smashed under hydrothermal conditions and spread over the flake particles as grapefruit-like particles (Figure 3b). Field emission-SEM (FE-SEM) images show that flake- or fiber-type particles with small branches of pineapple-like particles (inset in Figure 3c) are formed for a Ca/Y molar ratio of 25:75 (Figure 3c).

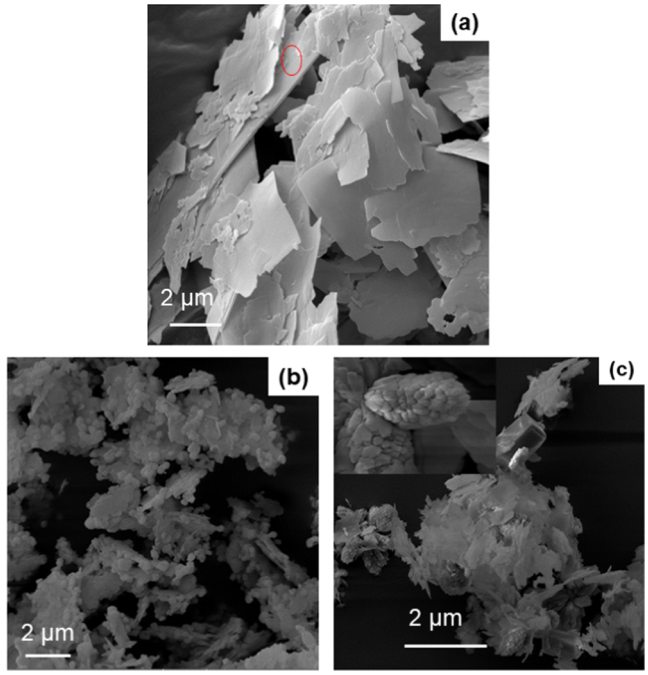

Figure 3. FE-SEM images of as-synthesized CaY LDH samples with Ca/Y molar ratios of (a) 75:25, (b) 50:50, and (c) 25:75.

The thickness of the sheets is approximately <1 nm. Note that almost all of the LDH crystallites overlap or are interconnected. Transmission electron microscopy (TEM) also confirmed the square-type layer structure of the composite materials. Figure 4a shows a typical CaY LDH nanoplate TEM image that is light compared to its periphery and darker when overlapping other nanoplates.

The morphologies of LDH materials have been examined with TEM and HRTEM. The results of the energy-dispersive

https://doi.org/10.1021/acsomega.1c03294
ACS Omega 2021, 6, 22909−22921

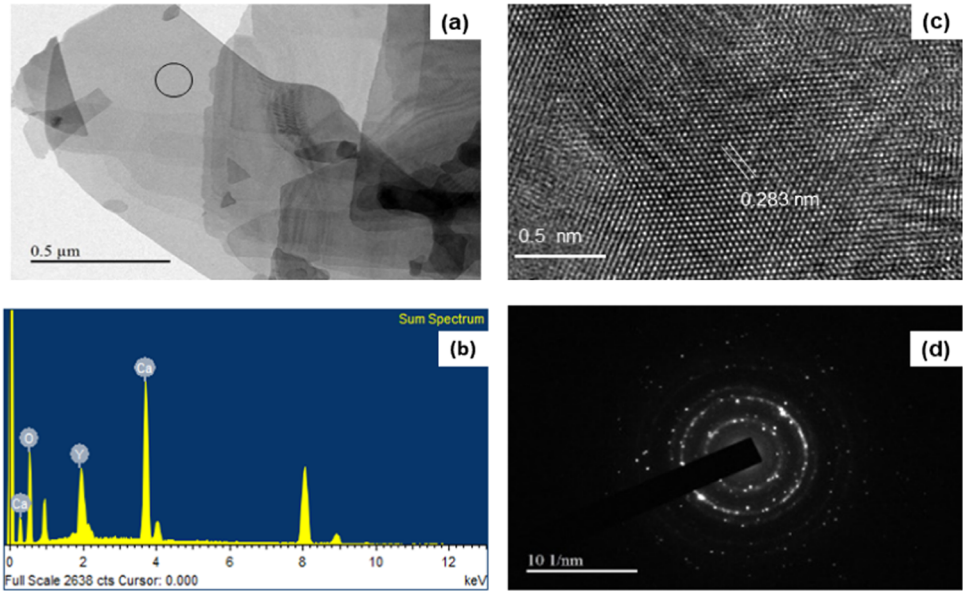

Figure 4. (a) TEM image of an as-synthesized CaY LDH sample with a Ca/Y molar ratio of 75:25; (b) energy-dispersive spectroscopy (EDS) spectrum for the region marked by a circle in (a); (c) the corresponding high-resolution transmission electron microscopy (HRTEM) image; (d) selected area electron diffraction (SAED) image.

X-ray (EDX) shown in Figure 4b show Y, Ca, and O. The EDX data was collected from a surface location marked with a circle in Figure 4a. The elemental map clearly shows that CaY is present in the nanoplates, which confirms that the as-prepared product is indeed a CaY LDH. The same elements were also found in other locations. The spacing between the fringes of the lattices was 0.283 ± 0.004 nm (Figure 4c). The sheet structure of the LDH was further examined using HRTEM. The pattern for selected area electron diffraction (SAED) (Figure 4d), taken from the sheet in Figure 4b,4d, gives the HRTEM image of a single-crystalline nanosheet. The pattern for selected electron diffraction (SAED) in Figure 4d contains broken rings, which suggests that the CaY LDHs consist of polycrystals with an oriented crystallographic axis.

Pore-Size Distribution. Figure 5A shows the pore structures of CaY LDH samples with molar ratios of (a) 75:25, (b) 50:50, and (c) 25:75 mol %. All of the data were obtained by evaluating N_2 adsorption−desorption isotherms.

The pores vary from large mesopores to macropores since the high P/P_0 range of 0.8−1.0 isotherms of all samples has been observed with an intense peak. The presence of slit-like pores is indicated by the isotherm form, which is typical of adsorption on a solid layer. For the samples in Figure 5a−c, the surface area was found to be 14, 9.28, and 5 m^2/g, respectively, suggesting a high surface area where the Ca content is high. The sheet-like particles have a higher surface area. McLaughlin et al. obtained a surface area of only 2 m^2/g for a MgAl LDH sample.[36] The pore-size distributions of the CaY LDH samples with molar ratios of 75:25 and 50:50 are both broad, in contrast to that of the sample with molar ratio 25:75. Thus, Figure 5B shows that samples (a) and (b) contain many more large mesopores and macropores than sample (c).

Based on the above results and discussion, CaY LDH with a molar ratio of 75:25 mol % showed the appropriate LDH formation structure, which had also a comparable high surface area and broad pore-size distribution. Therefore, the rest of the work was accomplished using CaY LDH with a molar ratio of 75:25.

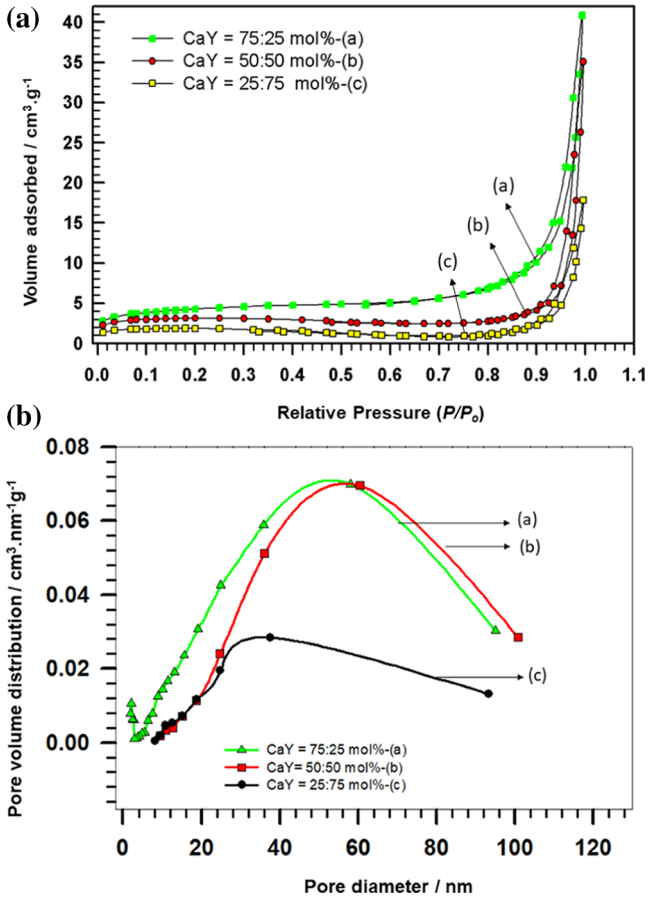

Figure 5. (A). N_2 adsorption/desorption isotherms for as-synthesized CaY LDH samples with Ca/Y molar ratios of (a) 75:25, (b) 50:50, and (c) 25:75. (B). The Barrett−Joyner−Halenda (BJH) pore-size distributions of as-synthesized CaY LDH samples with Ca/Y molar ratios of (a) 75:25, (b) 50:50, and (c) 25:75.

https://doi.org/10.1021/acsomega.1c03294
ACS Omega 2021, 6, 22909−22921

Table 2. Adsorption Results of CaY LDH toward the Individual Eight Ions (10 ppm)[a,b]

element	C_0 (ppm)	C_f (ppm)	initial pH	pH 24 h	removal %	q_m (mg/g)	K_d (mL/g)
Cr	10.11	0.030	6.22	7.20	99.703	10.08	3.36×10^5
Ni	10.56	0.350	5.86	7.63	96.68	10.21	2.92×10^4
Cu	11.00	0.300	6.18	7.47	97.27	10.7	3.57×10^4
As	10.65	0.010	6.90	7.92	99.90	10.64	1.06×10^6
Cd	10.69	0.400	7.10	7.50	96.25	10.29	2.57×10^4
Hg	9.89	0.506	6.50	7.65	94.88	9.384	1.85×10^4
Pb	10.65	0.060	6.30	7.04	99.43	10.59	1.77×10^5
Zn	10.02	0.08	6.80	7.12	99.20	9.92	1.24×10^5

[a]ion concentration: 10 ppm. Contact time: 8 h. [b]V = 30 mL; m (mass of the solid sample) = 0.03 g; V/m = 1000.

Heavy Metal Ion and Arsenic Uptake Capacity of CaY−CO_3^{2-} LDH. The assessment of CaY LDH's ability to remove heavy metal ions and arsenic from water was performed using the batch process at room temperature. Such studies were carried out with different ion concentrations. CaY LDH's ability to adsorb these ions has been tested for the distribution coefficient K_d. Two types of adsorption experiments were carried out: one for individual solutions of Cr^{3+}, Cd^{2+}, Ni^{2+}, Cu^{2+}, Zn^{2+}, Hg^{2+}, Pb^{2+}, and As^{3+}, and one for solutions containing all eight ions. Table 2 shows the results for the adsorption of different ions by CaY LDH. CaY LDH's ability to adsorb As^{3+}, Cr^{2+}, and Pb^{2+} is greater than that of other ions.

Nearly 100 percent elimination was achieved after 8 h of contact time, i.e., after this time, the concentrations of these ions decreased from starting values of about 10 ppm to about 1 ppb. K_d values >10×10^5 mL/g for As^{3+}, Cr^{3+}, and Pb^{2+} were obtained within 8 h. These findings contrast sharply with those for the other two metal ions, Cr^{3+} and Cu^{2+}. Also, CaY LDH's ability to adsorb Hg^{2+} and Ni^{2+} was weak, which is probably a good indicator of separating these ions. Table 3 shows the percentages of removal of all eight ions from a combined solution. The selectivity order of these ions is Ni^{2+} < Cr^{3+} < Pb^{2+} < Cu^{2+} < As^{3+} < Hg^{2+} < Cu^{2+}.

Table 3. Adsorption of CaY LDH toward the Eight Mixed Ions[a,b,c]

element	C_0 (ppm)	C_f (ppm)	removal (%)	K_d (mL/g)
Cr	10.25	0.987	90.37	9.39×10^3
Ni	10.65	1.500	85.91	6.10×10^3
Cu	10.98	0.978	91.09	1.02×10^4
As	10.87	0.999	90.81	9.88×10^3
Cd	11.25	1.200	89.33	8.38×10^3
Hg	10.96	0.985	91.01	1.01×10^4
Pb	9.89	0.967	90.23	9.23×10^3
Zn	10.30	0.97	90.58	9.62×10^3

[a]pH: 3.70 → 6.10. [b]ion concentration: 10 ppm. Contact time: 24 h. [c]V = 30 mL; m (mass of the solid sample) = 0.03 g; V/m = 1000.

The pH rises after the initial 8 h or maximum contact time, which is possibly due to the carbonate content of the limestone, which gives the sample buffer power (alkaline conditions) to the solution. Stumm et al. made the same observation, concluding that the presence of calcite balances the pH.[37] Calcium carbonate is added to the acidic aqueous solution, neutralization of acids occurs, and the concentration of dissolved calcium is increased. CaY−CO_3^{2-} shows the highest removal of heavy metals due to a combination of effects, i.e., the presence of $Y(OH)_2$, $CaCO_3$, and the LDH interlayer. As already mentioned, the presence of dissolved $CaCO_3$ increases the solution's pH above the solubility point. As a result, the metals are likely to precipitate as metal oxides or carbonates. These results seem to act in the same way as for the experiment on manganese.[21,22]

K_d values occur within the range of ~10^4 to 10^5 mL/g only for exceptional adsorbents.[35] CaY LDH can remove As present at trace levels and from highly concentrated solutions with outstanding efficiency. The capacities of CaY LDH for the adsorption of As^{3+} over the range of concentrations 1−10 ppm are shown in Table S6: above 99.9%, removal was achieved in all cases with a maximum adsorption capacity of ~500 mg/g.

We investigated the effects of varying the pH on the removal of various concentrations of Cr^{3+}, Cd^{2+}, Ni^{2+}, Cu^{2+}, Zn^{2+}, As^{3+}, Hg^{2+}, and Pb^{2+} from the sample solutions. In most cases, reducing the pH hinders ion removal (Tables S1−S8, S = supporting). On the other hand, higher pH values, i.e., above 7.00, enhance the removal. Only in the case of As^{3+} is the removal highly efficient over the pH range from 1.00 to 9.00 (Table S6), although high effectiveness was also observed in Pb^{2+}. The K_d value for the highly toxic Cr^{3+}, As^{5+}, and Pd^{2+} reaches ~10^7 mL/g, as shown in Tables S1, S6, and S8. The K_d values for the adsorption of Cr^{3+}, As, and Pd^{2+} are higher than those of other reported materials: KMS-2[38] and LHMS ($H_{2x}Mn_xSn_{3-x}S_6$) (10^3−10^6 mL/g),[39] marketable resins (~10^4 to 5.1×10^5 mL/g),[40] silane chelating fibers (3.0×10^5 to 3.8×10^6 mL/g),[41] and chalcogen-1 (9.2×10^6 to 1.6×10^7 mL/g).[42] The distribution coefficient K_d values on the order of ~10^4 to 10^5 mL/g arise only for extraordinary adsorbents.[22]

Furthermore, we have noted that the physical blend of CaO and Y_2O_3 with identical compositions is not as effective for the removal of As and other metal ions as CaY LDH. Using the same parameters as shown in Table 3, i.e., initial concentration of 10.12 ppm (pH 6.22), the removal was 65% in the case of As. This suggests that arsenate removal is more effective with CaY LDH, which is described in this study.

Sorption Isotherms for As and the Uptake Capacities of the Ions. We have shown that the newly produced CaY LDH material can rapidly reduce concentrations of toxic heavy metals to very low levels in aqueous solutions. The above results show that the highest selectivity of CaY LDH is that for As^{3+}. The adsorption of all of the highly toxic metal ions from the aqueous solution was found to be exceptionally rapid and highly selective, with more than 95% removal achieved within 30 min. The selectivity order for the ions being analyzed is as follows: Co^{2+}, Ni^{2+}, Zn^{2+} < Cd^{2+} ≪ Pb^{2+} < Cu^{2+} < Hg^{2+} < As^{3+} (Table 2). The distribution coefficient K_d values can exceed ~10^6 mL/g for Cr^{3+}, Pb^{2+}, and As^{3+}, which are highly toxic. It is important to note that only in As can K_d values reach ~10^7

https://doi.org/10.1021/acsomega.1c03294
ACS Omega 2021, 6, 22909−22921

mL/g (Table S6). Only in the case of As^{3+} is the removal highly efficient over the pH range from 1.00 to 9.00 (Table S6).

The material's overall adsorption efficiency was determined by performing adsorption-equilibrium experiments. The removal of As^{3+} by CaY LDH increases with increase in the concentrations (10−500 ppm). Greater than 98% removal of As^{3+} was achieved over a concentration range of 10−400 ppm; the K_d values were obtained from 4×10^4 to 3×10^7 mL/g. The maximum sorption potential (q_m) for As^{3+} was approximately 452 mg/g, which is surprisingly high compared to those of absorbers reported in other studies.[7,19,43,44] Very small As^{3+} concentrations, i.e., below 1 ppb, have been achieved, far below the appropriate standard for drinking water (2 ppb). These findings show that CaY LDH is a highly efficient filter for purification of water from harmful heavy metals and arsenic. The experimental data for As^{3+} can be presented in the form of a Langmuir isotherm. Based on this model, we infer that the As^{3+} ions on the adsorbent surface form a monolayer-type coating. No more adsorption will occur at this site as soon as an adsorption site is inaccessible or complete. The isothermic Langmuir model is given by

$$q = q_m \frac{bC_e}{1 + bC_e} \quad (1)$$

In the above equation, q (mg/g) represents the equilibrium adsorption capacity of As^{3+}, C_e (mg/L) represents the equilibrium concentration of As^{3+}, and q_m (mg/g) represents the theoretical optimum sorption capacity.

Figure 6 indicates the isothermic equilibrium adsorption varying from 0.02 to 400 ppm concentrations of equilibrium As^{3+}.

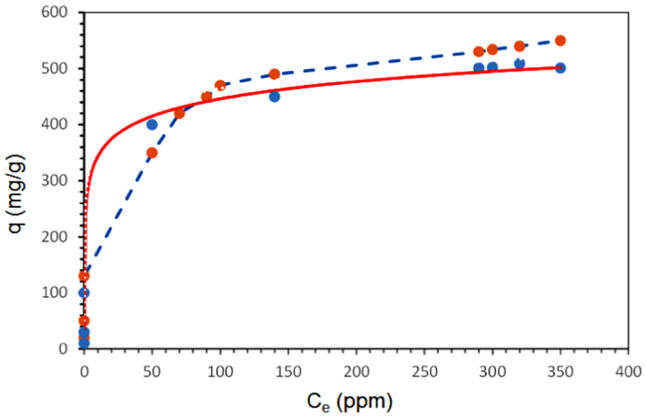

Figure 6. Isotherm for the sorption of As^{3+} by CaY LDH. The Langmuir equilibrium isotherm was derived from the As^{5+} equilibrium concentration (C_e) and plotted against the capacity q (mg/g).

The Langmuir model suits the data points well, and a q_m value of 501 mg/g has been found. The high correlation coefficient, $R^2 > 0.98$, indicates a strong match with the Langmuir model, indicating that As^{3+} forms monolayer adsorption on CaY LDH.[22,23] Two separate rate equations, namely the pseudo-first-order and pseudo-second-order mechanisms, were used to model the adsorption efficiency. To explore the adsorption rate and adsorption pathways before equilibrium, the kinetics of the adsorption of As^{3+} ions was also studied by CaY LDH. The adsorption of As^{3+} was found to be very fast and highly selective, as shown in Tables 4, S6, and Figure 7.

Table 4. Kinetics Data of As^{3+} Adsorption using CaY−CO_3^{2-} LDH[a,b]

time (min)	C_0 (ppm)	C_f (ppm)	removal (%)	q_t (mg/g)	K_d (mL/g)
5	20	0.73	96.35	19.27	2.64×10^4
30	20	0.068	99.66	19.932	2.93×10^5
60	20	0.049	99.75	19.951	4.07×10^5
120	20	0.002	99.99	19.998	1.00×10^7
180	20	0.0039	99.98	19.9961	5.13×10^6
240	20	0.003	99.98	19.997	6.67×10^6
300	20	0.002	99.99	19.998	1.00×10^7

[a]Ion concentration: 20 ppm. Contact time: 24 h. [b]V = 30 mL; m (mass of the solid sample) = 0.03 g; V/m = 1000.

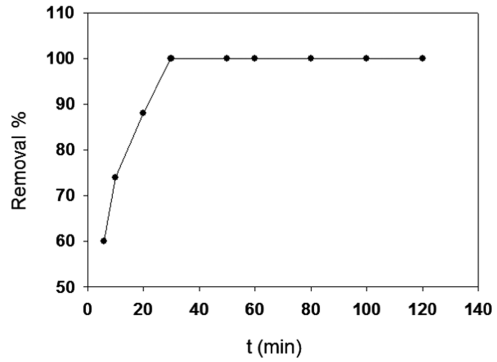

Figure 7. Adsorption kinetics curves for As^{3+}: removal % as a function of contact time. The measured maximal deviations for removal values were ±0.05, taking into account the averages of the five measurements.

CaY LDH shows an extremely effective ≥100% removal of As^{3+} within 30 min and K_d values of >104 mL/g (Table S6).

The experimental data were collected, calculated, and then compared. The two kinetic rate equations are as follows[44]

Pseudo-first-order

$$\ln(q_e - q_t) = \ln q_e - k_1 t \quad (2)$$

Pseudo-second-order

$$\frac{t}{q_t} = \frac{1}{k_2 q_e^2} + \frac{t}{q_e} \quad (3)$$

where the quantity of As^{3+} adsorbed per unit adsorbent mass is denoted by q_e (mg/g) at equilibrium and the quantity of As^{3+} adsorbed at time t is denoted by q_t (mg/g). k_1 (min^{-1}) = pseudo-first-order and k_2 (g/(mg min)) = pseudo-second-order adsorption rate constants, respectively.

By plotting $\ln(q_e - q_t)$ vs t, the value of k_1 can be calculated and that of k_2 by plotting t/qt vs t.

The kinetic parameters for Cr^{2+}, As^{3+}, Cd^{2+}, and Pb^{2+} are given in Table 5.

Calculated with the pseudo-second-order scale, the sorption capacities are relatively closer to the respective experimental values. The fit quality coefficient (R^2) is close to 1, indicating that CaY LDH may well explain the adsorption of these ions with a pseudo-second-order kinetic model, i.e., the adsorption process occurs via chemisorption.[45]

https://doi.org/10.1021/acsomega.1c03294
ACS Omega 2021, 6, 22909−22921

Table 5. Kinetics Parameters (Pseudo-Second-Order Model) for Adsorbing Metal Ions onto CaY−CO_3^{2-} LDH

	q_e	K_2	$q_{e,cal}$ (mg/g)	R^2
Cr^{3+}	18.20	0.30	19.00	0.97
As^{3+}	22.10	0.371	22.24	0.98
Cd^{2+}	17.00	0.298	17.47	0.99
Pb^{2+}	16.20	0.28	16.88	0.99

The effects of varying the hydrothermal reaction time and the temperature were also determined to optimize the morphology of CaY LDH and ensure the preparation of single-phase materials. Figure S1 shows the SEM images of the as-synthesized CaY LDH samples with a Ca/Y molar ratio of 75:25 prepared by using the hydrothermal method with various reaction times: (a) 36 h and (b) 12 h at 200 °C, and (c) 12 h at 120 °C. Very thin chef-knife-type particles and/or triangular-prism-type particles were obtained after 36 h of hydrothermal reaction at 200 °C (Figure S-1(a), S = supporting), whereas a layer-type morphology was obtained after 12 h at 200 °C (Figure S-1(b)); round thin particles were obtained after 12 h of hydrothermal reaction at 120 °C. Figure S-2 shows the XRD patterns and FT-IR spectra of these as-synthesized CaY LDH samples. All of the samples consist of mixed phases; therefore, none of these samples formed LDH-type materials. Besides, no standard layered structure was observed with a basal *d*-value of 0.76 nm.

X-Ray Photoelectron Spectroscopy (XPS) Analysis. The XPS analysis spectra in Figure 8 show the compositions and chemical states of the CaY LDH adsorbent with a molar ratio of 75:25 before and after exposure to As.

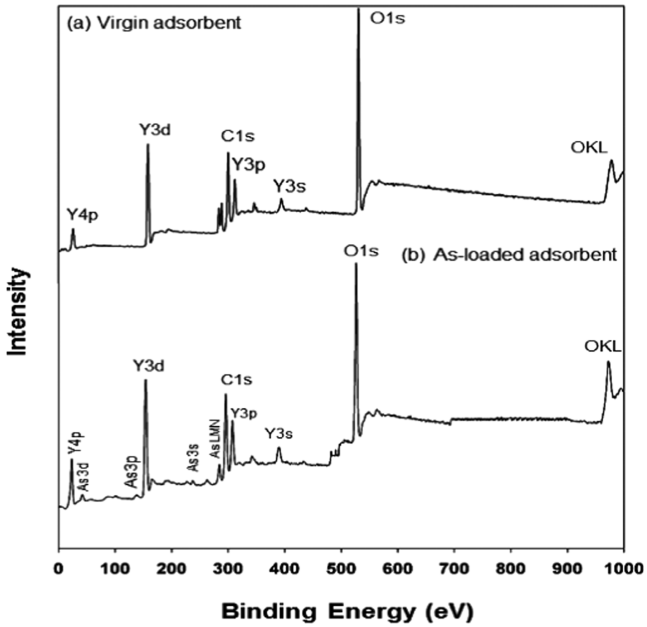

Figure 8. XPS wide scan spectra: (a) an as-synthesized adsorbent and (b) an As-loaded adsorbent.

The characteristic peaks of Y, Ca, O, and C demonstrate that the as-synthesized adsorbent surface contains these elements. Owing to spin−orbit splitting, the core-level spectrum of Y XPS 3d comprises two sublevels ($3d_{3/2}$ and $3d_{5/2}$). The spectrum Y $3d_{5/2}$ can be broken down into four components, as shown in Figure 9a. The Y 3d high-resolution spectrum

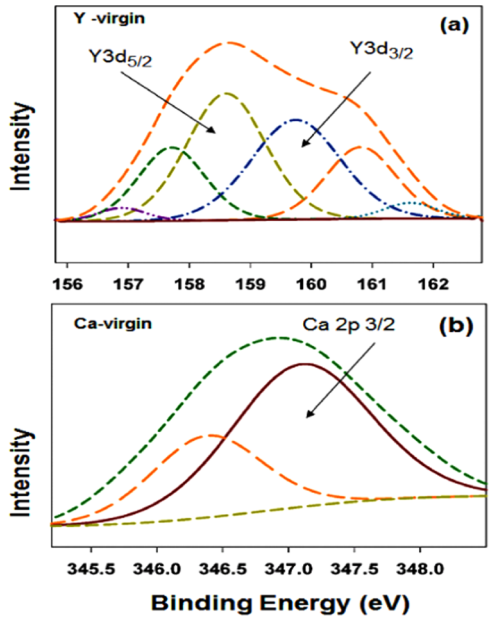

Figure 9. XPS spectra of the adsorbent: (a) Y 3d and (b) Ca 2p.

includes peaks for Y $3d_{5/2}$ at 156.9 eV and a further peak for Y $3d_{3/2}$ at 158.6 eV (Figure 9a). These results indicate that the yttrium is present in the adsorbent as Y^{3+}. The spectrum of the As-loaded sample (Figure 8b) contains peaks due to elemental yttrium, calcium, oxygen, and carbon as well as As. The appearance of peaks of As 3d, As 4p, As 3s, and As LMM shows the adsorption of arsenate particles. It is evident that the As(III) anions have replaced the OH^- groups and are bound by As−O−Y bonds during adsorption to hydrated yttrium oxide. Figure 8 displays the as-synthesized and As-loaded adsorbents with large XPS scan spectra.

These findings suggest that the CaY LDH content contains arsenic species. The surface concentration of As is 2.94 atom %, as obtained from the XPS spectrum. Figure 9b shows that the core-level spectrum of Ca XPS 2p is composed of two sublevels, i.e., $2p_{1/2}$ and $2p_{3/2}$, likely due to the spin−orbit break. The Ca $2p_{3/2}$ spectrum can be seen through three components: the first component is carbon, and the other two elements are attributed, respectively, to the absorbed species and water molecules.

The high energy-binding portion is probably due to adsorbed oxygen species like water and carbonates. Four component peaks are evident in the O 1s spectrum obtained with the high-resolution scan. Such peaks are due to yttrium oxide (YO), yttrium-bonded hydroxyl groups (Y−OH), and adsorbent-bonded water (H_2O) with 531.4, 531.9, and 533.1 eV binding energies, respectively (Figure 10a); the other low energy-binding portion is possibly due to CaO-associated oxygen. The high energy-binding portion of O 1s is likely due to the O species (for example, H_2O and CO_3^{2-}) attached to Y resulting from sample exposure to air and the hydrothermal cycle.

The core-level spectrum of As XPS 3d includes two sublevels, i.e., $3d_{3/2}$ and $3d_{5/2}$, likely due to the spin−orbit splitting. The As 3d peak is present at 45.5 eV and thus can be assigned to As(V). The other component is probably arsenic oxide (As_2O_3). The relative area ratios for the peaks were increased from 17.77 to 19.46% and 12.80 to 22.24%, respectively, because of M−O and H_2O after the metal ions

https://doi.org/10.1021/acsomega.1c03294
ACS Omega 2021, 6, 22909−22921

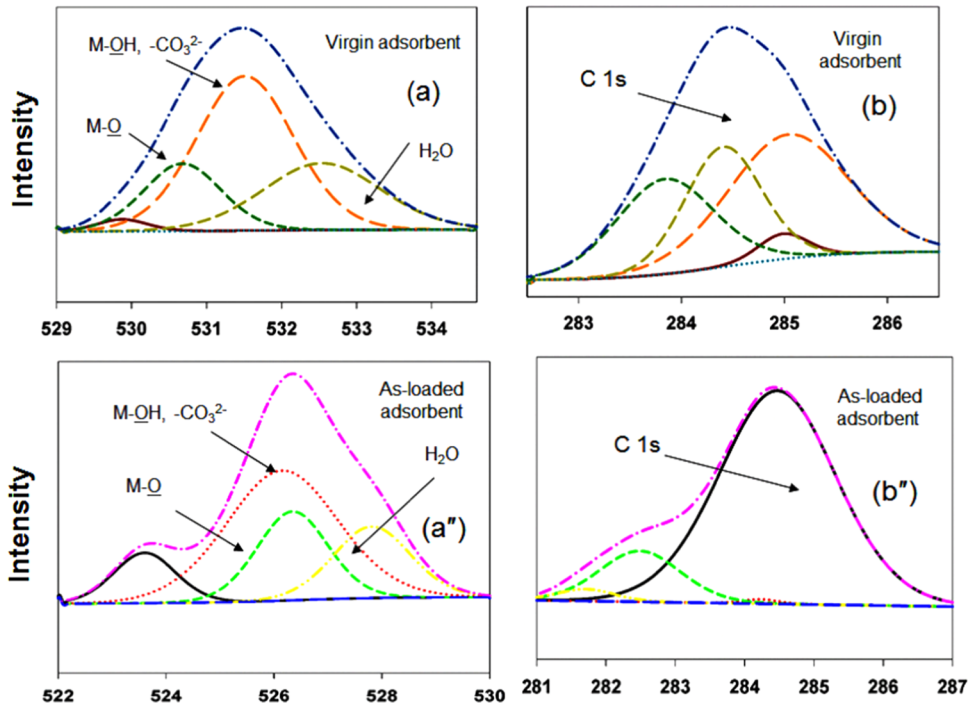

Figure 10. XPS spectra of an as-synthesized adsorbent: (a) O 1s and (b) C 1s; XPS spectra of an As-loaded adsorbent: (a″) O 1s and (b″) C 1s.

adsorption. On the other hand, the relative area ratio for the peaks was decreased from 69.43 to 58.30% because of M−OH and $-CO_3^{2-}$. This reduction in the peak area ratio shows that the OH^- and CO_3^{2-} groups engage in adsorption of As^{3+} on the adsorbent surface (Figure 10a″). Therefore, the hydroxyl groups on the adsorbent surface play a significant role in arsenic removal. The atmosphere and the precipitating agent NH_3CO_3 must be the origins of carbonate groups within the adsorbent. The spectrum of C 1s was broken down into five constituents, as shown in Figure 10b. The As-loaded sample spectrum was resolved into three component peaks (Figure 10a″). Except for the contamination caused by C−C (284.5 eV), the As-loaded sample C 1s XPS spectrum comprises three peaks. The peak of type CII is caused by carbon−oxygen bonds.

Table 6 displays the atomic ratios before and after adsorption of the adsorbents C, O, Y, Ca, and As, calculated

Table 6. Atomic Ratios for the Adsorbents Obtained with XPS

atomic ratio (%)	Y	Ca	O	C	As
virgin adsorbent	17.42	1.15	65.85	15.57	
As-loaded adsorbents	19.74	0.78	62.38	14.16	2.94

based on the XPS data. After the adsorption, the atomic percentage of arsenic on the surface has increased from 0 to 3.54%, and the atomic percentage of carbon on the surface has slightly decreased.

This result is a clear indication that As(III) can be adsorbed by the CaY−CO_3 and/or Y−$CaCO_3$ composite. The atomic fraction of O decreases after adsorption. This may be due to the replacement of As^{3+} ions for the OH^- and CO_3^{2-} groups on the adsorbent surface. Arsenic adsorption occurs through the formation of surface complexes by substituting arsenic ions for hydroxyl groups. Furthermore, the process of adsorption is influenced by the groups of carbonates and also by electrostatic interactions. Figure 6 displays the experimental results, which can be matched with the Langmuir and Freundlich adsorption isotherm models. The fitting with the Langmuir model has, according to the parameters mentioned in Table 4, a higher correlation coefficient (R^2 = 0.98) than that obtained with the Freundlich model (R^2 = 0.95), which implies that the Langmuir model is highly appropriate for the adsorption of As^{3+}.

Note also that when As(III) is adsorbed, the peaks Y $3d_{5/2}$ and Y $3d_{3/2}$ move marginally to higher binding energies. This result confirms that the As(III) anions are attached to hydrated yttrium oxide.[27] During adsorption of As(III), the compound Y−O−As is expected to form by exchange of hydroxyl groups on the adsorbent surface with As(III) anions in the solution. The reduction in the area ratio of $Y(OH)_3$ after adsorption might be due to the replacement of this group. It appears that the $Y(OH)_3$ formation in situ is responsible for the presence of $CaCO_3$ for arsenic removal from the water. It is important to note that $CaCO_3$ appears to be a great source of OH^{-1} compared with $Ca(OH)_2$. As mentioned above, OH^{-1} plays a crucial role in the removal of As^{3+}. Moreover, $CaCO_3$ can hold the pH stable because it releases OH^{-1} gradually.

Intercalation and precipitation play leading roles in eliminating heavy metal ions from radioactive sources. Adsorption by CaY LDH arises through intercalation into the interlayer spaces and precipitation of dissolved Ca^{2+} with anions. As(III) is almost eliminated by intercalation into the interlayers of the reconstructed CaY LDH at concentrations below 10 mg/L. We find less than 0.010 mg/L As^{3+} in the solution as left. Aziz and Zhang et al. studied manganese removal from water by limestone ($CaCO_3$) particles.[7,28] They showed that $CaCO_3$ is capable of removing more than 90% of heavy metals from 2 mg/L solutions at pH 8.5. There is another possibility, i.e., the formation of eutectic mixtures of

https://doi.org/10.1021/acsomega.1c03294
ACS Omega 2021, 6, 22909−22921

$CaCO_3-Y_2O_3-Ca(OH)_2$ or $CaCO_3-CaO-Y(OH)_3$,[27,45] which could play a part in extracting ions from metal.

Reusability and Regeneration Studies. After adsorption of the metal ions, XPS and TEM observations were also made. Solid samples were collected from suspension using a centrifuge, then dried. The materials retain their original laminar crystallite form after the As metal ion adsorption, suggesting good chemical stability (Figure 11b).

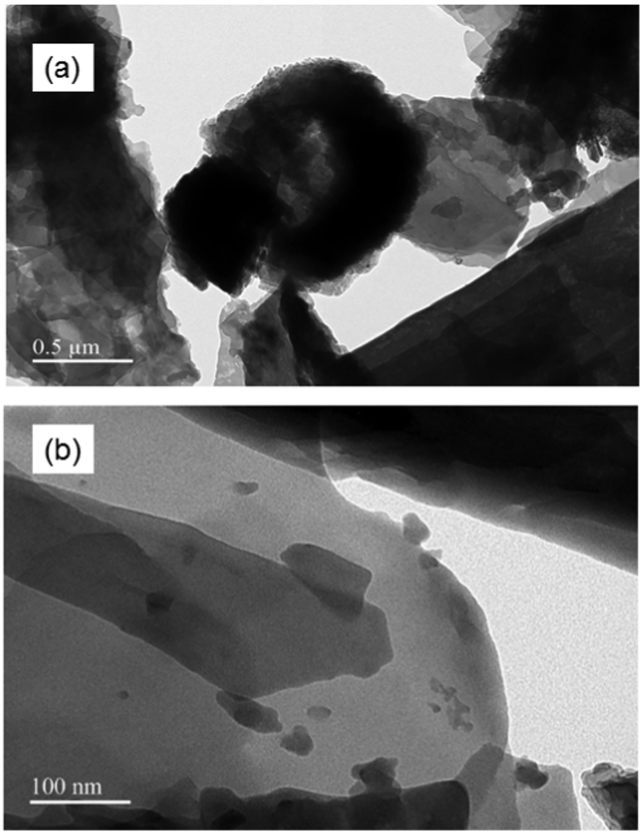

Figure 11. SEM images of solid CaY LDH samples after the adsorption of 10 ppm As^{3+}; TEM images at (a) low and (b) high magnification.

The typical TEM image in Figure 11a shows that some round particles are present after the adsorption of metal ions from aqueous media. Lijiao et al. reported several instances of the appearance of this type of particle after metal ion adsorption but did not explain the formation of this particle morphology.[19] It seems likely that such amorphous and/or dust-type particles agglomerate in the presence of H_2O during the metal ion adsorption process. The mass loss from leaching was small with respect to the total mass of the sorbent (<0.5 wt % leached). Heat treatment at 450 °C of the LDH after use was an efficient way to regenerate the products, with no change in the ability to remove As observed after five regeneration cycles. The potential reusability of CaY LDH over sorption−desorption repetitions as well as the possible recovery of arsenic from As-condensed desorbing liquid is shown by these results.

Finally, a comparison table (Table 7) with other LDH adsorbents has been prepared to understand CaY LDH's performance capability in water treatment.

CONCLUSIONS

A series of batch studies have been performed with various heavy metal solutions as well as arsenic solutions for investigating the adsorption potential of $CaY-CO_3^{-1}$ LDH at different pH values. Following are the conclusions of this investigation:

i. Nanosheets consisting of two-dimensional (2-D) nanomaterials made up of Ca^{2+} (Ca) and Y^{3+} (Y) cations and carbonate $[CO_3^{2-}]$ anions in the interlayer have been successfully synthesized, known as a layered double hydroxide (LDH). This is the first example of LDH materials based on Ca−Y. A very straightforward facile hydrothermal method has been used for the one-step synthesis.
ii. The mechanism of forming the lamellar $CaY-CO_3^{2-}$ LDHs depends on the molar ratio of Ca and Y and the reaction time and temperature. There are probably three mechanisms, viz. adsorption, precipitation, and carbonate and/or metal−OH bonding, that contribute to the extraction of metal ions and arsenic from solution.
iii. The capacities of CaY LDH for the adsorption of As^{5+} over the range of concentrations 1−10 ppm: above 99.9% removal was achieved. By using the absorbent CaY LDH, the concentrations of Pb^{2+} and As^{3+} ions can be decreased very rapidly from ppm to trace levels of as much as 1 ppb, which is far below the permissible drinking water level. Therefore, the composite materials $CaY-CO_3^{-1}$ LDH are excellent candidates for the rapid decontamination of heavy metals and arsenic-containing water.
iv. The selectivity order for the ions being analyzed is as follows: Co^{2+}, Ni^{2+}, $Zn^{2+} < Cd^{2+} \ll Pb^{2+} < Cu^{2+} < Hg^{2+} < As^{3+}$.
v. The kinetics of sorption systems fitted well to a pseudo-second-order model. In the case of As, K_d values can reach $\sim 10^7$ mL/g.
vi. Effective for mixed multi-ions removal.
vii. The fabricated materials have excellent chemical stability.
viii. This removal technique provides a straightforward method for remediating environmental damage by collecting and removing these metals from aqueous systems.

EXPERIMENTAL SECTION

Material Preparation. The CaY−carbonate layered double-hydroxide powders were prepared by the hydrothermal method. Y and Ca nitrate salts i.e., $Y(NO_3)_2{\cdot}6H_2O$ (Sigma Aldrich) and $Ca(NO_3)_2{\cdot}9H_2O$ (BDH Chemicals), were used as raw material. An appropriate amount of Y and Ca nitrate salts were liquefied using water. In this study, deionized water was used to dissolve for all types of inorganic salts. For the coprecipitation of metal ions, $(NH_4)_2CO_3$ was added into the salt solutions. The solutions were stirred vigorously for 12 h by keeping pH 8.5. The hydrothermal rector has a 500 cm^3 plastic container (Teflon bottle), which was placed into a steel vessel. The precursor suspension was transferred into the container. The hydrothermal reaction was carried out for 24 h at 200 °C after closing the vessel mouth. It was an almost airtight system. After the hydrothermal reaction, the reactor needs to be cooled down to 25 °C. Then, the white precipitation as the final product was collected and washed with CH_3CH_2OH (Merck

https://doi.org/10.1021/acsomega.1c03294
ACS Omega 2021, 6, 22909−22921

Table 7. Comparison of Adsorption Capacities of Heavy Metal Ions and As Removal with CaY LDH and Other Reported LDH Adsorbents

LDH sample	advantages	disadvantage	pH optimum	ref
CaY−CO_3^{2-} LDH	see the abstract, Introduction, and Conclusions.	a wide range of pH values needed to study	1.00−9.00 for As	this study
LDH nanoparticles (LDH-NP)	high anion exchangeability	synthesis time 24 h, extraction process took 2 h. Multicomponent removal is not performed. Kinetics of sorption systems fitted a pseudo-second-order model. Used another ligand	8	17
Zn/Al−CO_3^{2-} LDH	adsorption capacity 555.6 mg/g for Pb when the initial concentration was 500 mg/L	trace levels' (e.g., <5 ppb) extraction ability is not reported.	9.5	18
Mg/Al−CO_3 LDH or Ca-based LDH	efficiently removed As and phosphate	calcination needed 500 °C for 4 h; heavy metal ions removal was not examined. No XPS, SEM FT-IR analysis	8−9	20
MgAl (Sx)-NO_3 LDH	$K_d \sim 10^7$ mLg^{-1}	shaking time too long (3 days); polysulfide sensitivity to atmospheric oxygen. No As removal was examined	3	21
MgAl−MoS_4 LDH	$K_d \sim 10^7$ mLg^{-1}	medium-term instabilities associated with oxidation of the $[Sx]^{2-}$ species to $[SO_4]^{2-}$. No As removal was examined	2−10	22
Mg/Al LDH	LDH synthesis only, no heavy metal ions removal system reported	synthesis requires a long time (5−10 days)	7−8	24
Zn/Al−Cl LDH	nitrate removal	low desorption and poor regeneration for nitrate removal	6.00	45
LDH-humate hybrids	Cu was sorbed in greater amounts in all cases. Multicomponent removal performed.	recyclability not reported, and other toxic metals not studied		46
(Ca−Al−[Ca(EDTA)])-LDH	kinetics of all sorption systems fitted well to a pseudo-second-order model.	$[Ca(EDTA)]_2$ intercalation did not improve Ca−Al LDH performance, as the chelates were partially released.		47
$[Zn_4Al_2(OH)_{12}]$·EDTA·nH_2O	efficient for recovery of Cu(II). Chromate ions are efficiently adsorbed from water only by calcinated forms of LDHs.	no mixed ions removal, and kinetics studies were not provided. Does not remove U(VI) practically.	Lower pH is not effective	48

https://doi.org/10.1021/acsomega.1c03294
ACS Omega 2021, 6, 22909−22921

99.99% pure) and deionized H_2O three times to eliminate undesirable anions and dried at 120 °C for 12 h. Those powders are listed here as samples "as-synthesized".

Material Characterization. The Bruker D8 diffractometer (AXS Analytical X-ray Systems GmbH) was used to analyze the XRD pattern. XDR analysis was carried out using Cu Kα radiation (λ = 1.5405 Å) and maintaining an operating voltage of 40 kV and current of the diffractometer device of 50 mA. The XRD patterns were examined at a scanning velocity of 2 min^{-1} and with the 2θ values ranging from 5 to 80°. Using a Bruker FT-IR spectrometer (Bruker AXS Analytical X-ray Systems), the FT-IR spectra were collected. The sizes of the particles and morphological images were collected using FE-SEM (TESCAN LYRA3). The data were taken from the energy-dispersive X-ray (EDX) spectrum using an X-mass detector equipped with a Lyra3 TESCAN FE-SEM. For TEM images, a JEM 2011 (JEOL Inc.) was used, operated by a CCD camera working at 200 kV. A NOVA-1200 device (JEOL) was used to assess the Brunauer−Emmett−Teller (BET) data, for example, pore size and surface area. The N_2 adsorption isotherms were obtained in liquid N_2. Before the BET experiments, the powders were evacuated for 3 h at 200 °C. After that, this experiment was carried out a heating rate of 5 °C/min from 25 to 600 °C under a dry N_2 atmosphere. To examine the chemical compositions of the samples, X-ray photoelectron spectroscopy (XPS) (ESCALAB-250, Thermo-VG Scientific) with Al-Kα radiation (1486.6 eV) instrument was used. The XPS spectra were collected for all samples at 25 °C with a pressure of 5 × 10^{-10} m bar. A Shimadzu thermal analyzer (TA-50) was used to collect the thermogravimetric analysis (TGA) data. For each TGA measurement, about 10 mg of sample was used. The heating rate was maintained at 10 °C/min from 25 to 600 °C under a dry N_2 atmosphere. The melting and freezing points and the latent heat value of the samples were obtained by DSC-Q2000. DSC data were collected by heating 8.5 mg of sealed samples in an Al pan. DSC data were collected under the argon gas atmosphere, and the gas flow rate was maintained at 20 mL/min with a heating rate of 5 °C/min. For the thermal conductivity of the powders, round-type disk samples were prepared, and then a TCi Conductivity Analyzer, Canada, was used to measure the thermal conductivity. This equipment used the modified transient plane source and a method of C-Therm Technologies.

Experiments on Removing Heavy Metals. The metal ions adsorption from aqueous solutions was measured using the batch process by changing the concentrations of the heavy metal ions. Similar experiments were carried out with solutions containing 0.2, 0.5, 1, 5, 10, and 20 ppm As^{3+} (prepared from a standard solution of the solute: arsenic acid H_3AsO_4, matrix HNO_3 = 0.5 mg/L, c(As) = 1000 ± 5 mg^{-1}, BDH Lab. Poole, BH 151TD, England). The metal ions Co^{2+}, Ni^{2+}, Cu^{2+}, Zn^{2+}, As^{3+}, Pb^{2+}, Cd^{2+}, and Hg^{2+} were present in the solution as nitrate salts. Then, the metal ions solutions were mixed with solid sorbents for a certain time and centrifugation was performed at 6000 rpm for 3 min. Using inductively coupled plasma-mass spectroscopy (XSE RIES-II), the metal concentrations in the supernatant solutions were measured. The adsorptive potential was determined from the variations between the mother solution's metal concentrations and those of the supernatant solutions.

The equation $K_d = (V[(C_0 - C_f)/C_f])/m$ represents the coefficient of distribution, where C_0 and C_f are the initial and equilibrium concentrations of M^{n+} ppm, V is the volume of the solution (mL), and m is the solid quantity (g). The amount of extraction was determined using the following equation:

$$100 \times (C_0 - C_f)/C_o$$

The removal capacity (q_m) is determined according to the equation

$$q_m = 10^{-3} \times (C_0 - C_f)V/m$$

To assess the selectivity of the adsorbents for Cu^{2+}, Hg^{2+}, and Ag+, experiments were carried out on solutions containing all of them together. Solutions of each ion were combined with other concentrations of CaY LDHs (0.01 and 0.005 g) at a concentration of approximately 10 ppm (about 30 ppm in total). The removal capacities of the ions Hg^{2+}, Ag+, Cu^{2+}, and Pb^{2+} were calculated by the batch process at 25 °C (V/m = 860−1000 mL/g), and the contact time was 24 h. The data collected were used to assess the isothermic sorption. All of the experiments were carried out in triplicate with the reproducibility within ±3%.

Adsorption Kinetic Study. Kinetic studies were conducted on the adsorption of As^{3+} ions over different periods (5−300 min). 0.030 g of the solid CaY LDH sample was taken into a 50 mL tube in each experiment, and then 30 mL of aqueous solution (containing the 20−30 ppm ion) was introduced (V/m = 1000 mL/g). Each suspension was centrifuged at specified time intervals and 2 mL of the supernatant solution was analyzed to determine the ion content using ICP-MS. The data were processed with Plasma Lab windows platform software.

■ ASSOCIATED CONTENT

Supporting Information

The Supporting Information is available free of charge at https://pubs.acs.org/doi/10.1021/acsomega.1c03294.

FE-SEM images; XRD patterns of SEM images of as-synthesized CaY LDH samples with a Ca:Y molar ratio of 25:75 prepared by using the hydrothermal method for two different reaction times: (a) 36 h and (b) 12 h at 200 °C and (c) 12 h at 120 °C (Figure S.1); As-synthesized CaY LDH with a Ca:Y molar ratio of 25:75 prepared by using the hydrothermal method for two different reaction times: (a) 36 h and (b) 12 h at 200 °C and (c) 12 h at 120 °C, and FT-IR spectra (d), (e), and (f) of the same samples (Figure S.2); absorption data of different Concentration (Tables S.1−S.8) (PDF)

■ AUTHOR INFORMATION

Corresponding Author

Md. Hasan Zahir − *Interdisciplinary Research Center for Renewable Energy and Power Systems (IRC-REPS), Research Institute, King Fahd University of Petroleum & Minerals, (KFUPM), Dhahran 31261, Saudi Arabia;* orcid.org/0000-0002-6752-9318; Email: hzahir@kfupm.edu.sa

Authors

Kashif Irshad − *Interdisciplinary Research Center for Renewable Energy and Power Systems (IRC-REPS), Research Institute, King Fahd University of Petroleum & Minerals, (KFUPM), Dhahran 31261, Saudi Arabia;* orcid.org/0000-0001-6493-0969

Mohammad Mizanur Rahman − *Interdisciplinary Research Center for Advanced Materials, KFUPM, Dhahran 31261, Saudi Arabia;* orcid.org/0000-0002-9302-3185

M. Nasiruzzaman Shaikh − *Interdisciplinary Research Center for Hydrogen and Energy Storage (IRC-HES), KFUPM, Dhahran 31261, Saudi Arabia;* orcid.org/0000-0002-9549-6322

Mohammad Mominur Rahman − *Department of Electrical Engineering, King Saud University, Riyadh 11495, Saudi Arabia;* orcid.org/0000-0002-9703-1748

Complete contact information is available at: https://pubs.acs.org/10.1021/acsomega.1c03294

Notes

The authors declare no competing financial interest.

■ ACKNOWLEDGMENTS

The authors would like to acknowledge the support provided by the Deanship of Scientific Research (DSR) at King Fahd University of Petroleum & Minerals (KFUPM) by funding this work through the project number: IN171036.

■ REFERENCES

(1) Shannon, M. A.; Bohn, P. W.; Elimelech, M.; Georgiadis, J. G.; Marĩas, B. J..; Mayes, A. M. Science and technology for water purification in the coming decades. *Nature* **2008**, *452*, 301−310.

(2) Karim, M. M. Arsenic in Groundwater and Health Problems in Bangladesh. *Water Res.* **2000**, *34*, 304−310.

(3) WHO (World Health Organization). *World Health Organization*: Geneva, 1993, Vol. *1*, p 45.

(4) Meranger, J. C.; Subramanian, K. S.; McCurdy, R. F. Arsenic in Nova Scotian groundwater. *Sci. Total Environ.* **1984**, *39*, 49−55.

(5) Jain, C. K.; Ali, I. Arsenic: occurrence, toxicity and speciation techniques. *Water Res.* **2000**, *34*, 4304−4312.

(6) Schwarzenbach, R. P.; Escher, B. I.; Fenner, K.; Hofstetter, T. B.; Johnson, C. A.; von Gunten, U.; Wehrli, B. The Challenge of Micropollutants in Aquatic Systems. *Science* **2006**, *313*, 1072−1076.

(7) Aziz, H. A.; Adla, M. N.; Ariffin, K. S. Heavy metals (Cd, Pb, Zn, Ni, Cu and Cr(III)) removal from water in Malaysia: Post treatment by high quality limestone. *Bioresour. Technol.* **2008**, *99*, 1578−1583.

(8) Luong, V. T.; Edgardo, E.; Kurz, Ca∼nas.; Ulrich, H.; Tran, L. L.; Hoinkis, J. Iron-based subsurface arsenic removal technologies by aeration: A review of the current state and future prospects. *Water Res.* **2018**, *133*, 110−122.

(9) Borho, M.; Wilderer, P. Optimized removal of arsenate(III) by adaptation of oxidation and precipitation processes to the filtration step. *Water Sci. Technol.* **1996**, *34*, 25−31.

(10) Hansen, H. K.; Nunez, P.; Grandon, R. Electrocoagulation as a remediation tool for wastewaters containing arsenic. *Miner. Eng.* **2006**, *19*, 521−524.

(11) Han, B.; Runnells, T.; Zimbron, J.; Wickramasinghe, R. Arsenic removal from drinking water by flocculation and microfiltration. *Desalination* **2002**, *145*, 293−298.

(12) Kim, J.; Benjamin, M. M. Modeling a novel ion exchange process for arsenic and nitrate removal. *Water Res.* **2004**, *38*, 2053−2062.

(13) Chuang, C. L.; Fan, M.; Xu, M.; Brown, R. C.; Sung, S.; Saha, B.; Huang, C. P. Adsorption of arsenic (V) by activated carbon prepared from oat hulls. *Chemosphere* **2005**, *61*, 478−483.

(14) Malana, M. A.; Qureshi, R. B.; Ashiq, M. N. Adsorption studies of arsenic on nano aluminium doped manganese copper ferrite polymer (MA, VA, AA) composite: Kinetics and mechanism. *Chem. Eng. J.* **2011**, *172*, 721−727.

(15) Wang, C.; Liu, H.; Zhang, Y.; Zou, C.; Anthony, E. J. Anthony Review of arsenic behavior during coal combustion: Volatilization, transformation, emission and removal technologies. *Prog. Energy Combust. Sci.* **2018**, *68*, 1−28.

(16) Zhang, G.; Liu, H.; Liu, R.; Qu, J. Removal of phosphate from water by a Fe-Mn binary oxide adsorbent. *J. Colloid Interface Sci.* **2009**, *335*, 168−174.

(17) Kuroda, Y.; Miyamoto, Y.; Hibino, M.; Yamaguchi, K.; Mizuno, N. Tripodal Ligand-Stabilized Layered Double Hydroxide Nanoparticles with Highly Exchangeable CO32-. *Chem. Mater.* **2013**, *25*, 2291−2296.

(18) Wang, L.; Wang, X.; Li, J.; Feng, X.; Wang, Y. Silica Aerogel-supported Hydrozincite and Carbonate-intercalated Hydrotalcite for High-efficiency Removal of Pb(II) Ions by Precipitation Transformation Reactions. *Nanoscale Res. Lett.* **2017**, *12*, No. 549.

(19) Yu, Y.; Yu, L.; Sun, M.; Chen, J. P. Facile synthesis of highly active hydrated yttrium oxide towards arsenate adsorption. *J. Colloid Interface Sci.* **2016**, *474*, 216−222.

(20) Xu, Y.; Dai, Y.; Zhou, J.; Xu, Z. P.; Qian, G.; Max Lu, G. Q. Removal efficiency of arsenate and phosphate from aqueous solution using layered double hydroxide materials: intercalation vs. precipitation. *J. Mater. Chem.* **2010**, *20*, 4684−4691.

(21) Ma, S.; Shim, Y.; Islam, S. M.; Subrahmanyam, K. S.; Wang, P.; Li, H.; Wang, S.; Yang, X.; Kanatzidis, M. G. Efficient Hg Vapor Capture with Polysulfide Intercalated Layered Double Hydroxides. *Chem. Mater.* **2014**, *26*, 5004−5011.

(22) Ma, L.; Wang, Q.; Islam, S. M.; Liu, Y.; Ma, S.; Kanatzidis, M. G. Highly Selective and Efficient Removal of Heavy Metals by Layered Double Hydroxide Intercalated with the MoS42− Ion. *J. Am. Chem. Soc.* **2016**, *138*, 2858−2866.

(23) Ma, S.; Chen, Q.; Li, H.; Wang, P.; Islam, S. M.; Gu, Q.; Yang, X.; Kanatzidis, M. G. Highly selective and efficient heavy metal capture with polysulfide intercalated layered double hydroxides. *J. Mater. Chem. A* **2014**, *2*, 10280−10289.

(24) Xu, Z. P.; Lu, G. Q. Hydrothermal Synthesis of Layered Double Hydroxides (LDHs) from Mixed MgO and Al2O3: LDH Formation Mechanism. *Chem. Mater.* **2005**, *17*, 1055−1062.

(25) Lide, D. R. *Handbook of Chemistry and Physics*; Chapman & Hall: New York, 1999.

(26) Xu, Z. P.; Zhang, J.; Adebajo, M. O.; Zhang, H.; Zhou, C. Review Article- Catalytic applications of layered double hydroxides and derivatives. *Appl. Clay Sci.* **2011**, *53*, 139−150.

(27) García-García, J. M.; Pérez-Bernal, M. E.; Ruano-Casero, R. J.; Rives, V. Chromium and yttrium-doped magnesium aluminum oxides prepared from layered double hydroxides. *Solid State Sci.* **2007**, *9*, 1115−1125.

(28) Zhang, T.; Zhao, B.; Bai, H.; Wang, W.; Zhang, Q. Enhanced arsenic removal from water and easy handling of the precipitate sludge by using FeSO4 with CaCO3 to Ca(OH)2. *Chemosphere* **2019**, *231*, 134−139.

(29) Zhipan, W.; Jun, L.; Yalei, Z.; Gang, C.; Shengnan, H.; Jin, C.; Rui, X.; Yin-an, M.; Yingru, W.; Rong, C. Facile inverse micelle fabrication of magnetic ordered mesoporous iron cerium bimetal oxides with excellent performance for arsenic removal from water. *J. Hazard. Mater.* **2020**, *383*, No. 121172.

(30) Miyata, S. Anion-exchange properties of hydrotalcite-like compounds. *Clay Clay Miner.* **1983**, *31*, 305−311.

(31) Bookin, A. S.; Cherkashin, V. I.; Drits, V. A. Polytype diversity of the hydrotalcite-like minerals ii. determination of the polytypes of experimentally studied varieties. *Clay Clay Miner.* **1993**, *41*, 558−564.

(32) Newman, S. P.; Jones, W.; O'Connor, P.; Stamires, D. N. Synthesis of the 3R2 polytype of a hydrotalcite-like mineral. *J. Mater. Chem.* **2002**, *12*, 153−155.

(33) Vicente, P.; Pérez-Bernal, M. E.; Ruano-Casero, R. J.; Ananias, D.; Almeida Paz, F. A.; Rocha, J.; Rives, V. Luminescence properties of lanthanide-containing layered double hydroxides. *Microporous Mesoporous Mater.* **2016**, *226*, 209−220.

(34) Nakamoto, K. *Infrared and Raman Spectra of Inorganic and Coordination Compounds, Part A, Theory and Applications in Inorganic Chemistry*, 6th ed.; Wiley: Hoboken, 2009.

(35) Cavani, F.; Trifirò, F.; Vaccari, A. Hydrotalcite-type anionic clays: preparation, properties and applications. *Catal. Today* **1991**, *11*, 173−301.
(36) McLaughlin, W. J.; White, J. L.; Hem, S. L. Influence of Heterocoagulation on the Formation of Hydrotalcite in Mixed Suspensions of Magnesium Hydroxide and Aluminum Hydroxycarbonate. *J. Colloid Interface Sci.* **1994**, *165*, 41−52.
(37) Stumm, W.; Morgan, J. J. *Aquatic Chemistry: An Introduction Emphasizing Chemical Equilibria in Natural Waters*, 2nd ed.; John Wiley & Sons Ltd: New York, 1981.
(38) Hassanzadeh Fard, Z.; Malliakas, C. D.; Mertz, J. L.; Kanatzidis, M. G. Direct Extraction of Ag+ and Hg2+ from Cyanide Complexes and Mode of Binding by the Layered K2MgSn2S6 (KMS-2). *Chem. Mater.* **2015**, *27*, 1925−1928.
(39) Manos, M. J.; Petkov, V. G.; Kanatzidis, M. G. H2xMnxSn3-xS6 (x = 0.11-0.25): A novel reusable sorbent for highly specific mercury capture under extreme pH conditions. *Adv. Funct. Mater.* **2009**, *19*, 1087−1092.
(40) Yantasee, W.; Warner, C. L.; Sangvanich, T.; Addleman, R. S.; Carter, T. G.; Wiacek, R. J.; Fryxell, G. E.; Timchalk, C.; Warner, M. G. Removal of heavy metals from aqueous systems with thiol functionalized superparamagnetic nanoparticles. *Environ. Sci. Technol.* **2007**, *41*, 5114−5119.
(41) Liu, C. Q.; Huang, Y. Q.; Naismith, N.; Economy, J.; Talbott, J. Economy, Novel Polymeric Chelating Fibers for Selective Removal of Mercury and Cesium from Water. *J. Environ. Sci. Technol.* **2003**, *37*, 4261−4268.
(42) Bag, S.; Trikalitis, P. N.; Chupas, P. J.; Armatas, G. S.; Kanatzidis, M. G. Porous semiconducting gels and aerogels from chalcogenide clusters. *Science* **2007**, *317*, 490−493.
(43) Liu, T.; Yang, M.; Wang, T. X.; Yuan, Q. P. Prediction strategy of adsorption equilibrium time based on equilibrium and kinetic results to isolate taxifolin. *Ind. Eng. Chem. Res.* **2012**, *51*, 454−463.
(44) Bhattacharya, A. K.; Naiya, T. K.; Mandal, S. N.; Das, S. K. Adsorption, kinetics and equilibrium studies on removal of Cr(VI) from aqueous solutions using different low-cost adsorbents. *Chem. Eng. J.* **2008**, *137*, 529−541.
(45) Islam, M.; Patel, R. Synthesis and physicochemical characterization of Zn/Al chloride layered double hydroxide and evaluation of its nitrate removal efficiency. *Desalination* **2010**, *256*, 120−128.
(46) González, M. A.; Pavlovic, I.; Barriga, C. Cu(II), Pb(II) and Cd(II) sorption on different layered double hydroxides. A kinetic and thermodynamic study and competing factors. *Chem. Eng. J.* **2015**, *269*, 221−228.
(47) Rojas, R. Copper, lead and cadmium removal by Ca Al layered double hydroxides. *Appl. Clay Sci.* **2014**, *87*, 254−259.
(48) Pshinko, G. N. Layered Double Hydroxides as Effective Adsorbents for U(VI) and Toxic Heavy Metals Removal from Aqueous Media. *J. Chem.* **2013**, No. 347178.

https://doi.org/10.1021/acsomega.1c03294
ACS Omega 2021, 6, 22909−22921